AGU PUBLICATIONS

Geophysical Research Letters

RESEARCH LETTER
10.1002/2016GL071978

Key Points:
- Local and remote feedbacks between low clouds, SST, and large-scale circulation sustain PDV
- Changes in SWCRE confined to eastern subtropical Pacific reproduce observed cool SSTs and U.S. drought
- Novel coupling strategy utilized observed patterns of SWCRE to examine low clouds in coupled models

Supporting Information:
- Supporting Information S1

Correspondence to:
R. J. Burgman,
rburgman@fiu.edu

Citation:
Burgman, R. J., B. P. Kirtman, A. C. Clement, and H. Vazquez (2017), Model evidence for low-level cloud feedback driving persistent changes in atmospheric circulation and regional hydroclimate, *Geophys. Res. Lett.*, *44*, 428–437, doi:10.1002/2016GL071978.

Received 17 NOV 2016
Accepted 19 DEC 2016
Accepted article online 21 DEC 2016
Published online 13 JAN 2017

Model evidence for low-level cloud feedback driving persistent changes in atmospheric circulation and regional hydroclimate

Robert J. Burgman[1], Ben P. Kirtman[2], Amy C. Clement[2], and Heather Vazquez[1]

[1]Department of Earth and Environment, Florida International University, Miami, Florida, USA, [2]Rosenstiel School of Marine and Atmospheric Science, University of Miami, Coral Gables, Florida, USA

Abstract Recent studies suggest that low clouds in the Pacific play an important role in the observed decadal climate variability and future climate change. In this study, we implement a novel modeling experiment designed to isolate how interactions between local and remote feedbacks associated with low cloud, SSTs, and the large-scale circulation play a significant role in the observed persistence of tropical Pacific SST and associated North American drought. The modeling approach involves the incorporation of observed patterns of satellite-derived shortwave cloud radiative effect (SWCRE) into the coupled model framework and is ideally suited for examining the role of local and large-scale coupled feedbacks and ocean heat transport in Pacific decadal variability. We show that changes in SWCRE forcing in eastern subtropical Pacific alone reproduces much of the observed changes in SST and atmospheric circulation over the past 16 years, including the observed changes in precipitation over much of the Western Hemisphere.

1. Introduction

To understand the impact of decadal variability in the Pacific on global and regional climate, one only needs to look at the last 16 years. In the late 1990s the tropical Pacific sea surface temperatures (SSTs) transitioned to a La Niña-like cool phase, reversing the El Niño-like conditions that had persisted since the late 1970s. The cool conditions in the tropical Pacific have been linked to changes in regional sea level rise [*Hamlington et al.*, 2013], strengthening of the large-scale atmospheric circulation [*Chen et al.*, 2008; *Burgman et al.*, 2008b], a reduction in the rate of increase in the global mean surface temperature [*Meehl et al.*, 2011; *England et al.*, 2014], and persistent drought conditions in North America [*Hoerling and Kumar*, 2003; *Schubert et al.*, 2004, 2009; *Seager et al.*, 2005, 2008; *Burgman and Jang*, 2015].

For decades, researchers have investigated the spatial and temporal characteristics of decadal variability in the Pacific over the past century and its influence on the ocean and atmospheric circulation, regional climate, and marine ecosystems. Using surface observations and differing metrics, several authors identified several "regime shifts" in the Pacific over the past century occurring in the mid-1920s, the mid-1940s, and in the late 1970s [*Trenberth and Hurrell*, 1994; *Mantua et al.*, 1997; *Zhang et al.*, 1997; *Power et al.*, 1999]. The SST structure of Pacific decadal variability (PDV) is characterized by a broad triangular pattern in the tropical Pacific surrounded by opposite anomalies in the midlatitudes of the central and western Pacific Basin. In the late 1990s and early 2000s the Pacific transitioned to the cool La Niña-like phase of the oscillation [*Chen et al.*, 2008; *Burgman et al.*, 2008b; *Jo et al.*, 2013]. This cool PDV pattern persisted until very recently, when a large pattern of warming expanded throughout much of the Northeast Pacific, indicating a possible shift back to the positive phase.

Concurrent with the recent cool PDV phase, North America has experience persistent arid conditions punctuated by several unprecedented regional droughts. Several modeling studies have attributed persistent drought in North America with a La Niña-like PDV SST pattern [*Hoerling and Kumar*, 2003; *Seager et al.*, 2005, 2008; *Schubert et al.*, 2009; *Burgman et al.*, 2010]. In addition to the well-documented boreal winter Pacific North American response [*Trenberth et al.*, 1998], *Seager et al.* [2003] identified a zonally symmetric shift in the storm tracks associated with persistent changes in the tropical Pacific SSTs as a mechanism for persistent changes in precipitation in the Western Hemisphere.

Several theories for the mechanisms behind PDV have been proposed and fall into three broad categories involving: (1) ocean-atmosphere interactions in the North Pacific [*Barnett et al.*, 1999; *Pierce et al.*, 2000], (2) tropical-extratropical interactions including oceanic and atmospheric teleconnections [*Lau and Nath*, 1994;

Wang and Weisberg, 1998; *Kleeman et al*., 1999; *McPhaden and Zhang*, 2002; *Pierce*, 2002], or (3) internal tropical dynamics [*Knutson and Manabe*, 1998; *Kirtman*, 1997; *Jin*, 2001]. Within these categories there is still debate as to the relative importance of oceanic teleconnections that transfer signals from the midlatitudes to the tropics via subduction or waves, the role of the shallow meridional overturning circulation, the relative importance of the northern and southern oceans [*Galanti and Tziperman*, 2003; *Giese et al*., 2002], and the role of stochastic forcing [*Kirtman and Schopf*, 1998; *Yeh and Kirtman*, 2006; *Burgman et al*., 2008a; *Kirtman et al*., 2011]. Still others suggest that PDV may be driven by thermodynamics, or atmospheric dynamics and air-sea interactions [*Clement et al*., 2011; *Chen and Wallace*, 2015], or as a residual of interannual variability in the tropical Pacific [*Schopf and Burgman*, 2006].

1.1. Are the Large-Scale Pacific Circulation and North American Hydroclimate Changes Linked to Low Cloud Variability in the Eastern Subtropical Pacific?

Several recent studies have concluded that feedbacks between SSTs, low clouds in the eastern subtropical Pacific, and the large-scale atmospheric circulation in the Pacific may play an important role in the persistence of PDV [*Burgman et al*., 2008b; *Clement et al*., 2009; *Bellomo et al*., 2014]. Low clouds in the eastern subtropical Pacific have a large negative cloud radiative effect (CRE) due to their high albedo and weak greenhouse effect [*Hartmann et al*., 1992]. Here "low cloud" includes marine stratiform clouds such as ordinary stratocumulus, cumulus under stratocumulus, and fair and bad weather stratus. These clouds occur in shallow marine boundary layers over cool SSTs and under regions of large-scale subsidence. Low clouds are positively correlated to the strength of the capping inversion and negatively correlated to the underlying SST [*Klein et al*., 1995; *Wood and Bretherton*, 2006; *Clement et al*., 2009]. Thus, for a local reduction in SST or increase in potential temperature above the temperature inversion, lower tropospheric stability (LTS) and low cloud increase forcing a reduction of incoming SW radiation and SST.

In addition to local feedbacks, low clouds have also been observed to coincide with basin-wide changes in the coupled ocean-atmospheric circulation on decadal timescales. Using satellite and surface-based observations, *Burgman et al*. [2008b] and *Clement et al*. [2009] showed that changes in the variables controlling low cloud amount in the eastern subtropical Pacific including lower tropospheric stability (LTS), SST, sea level pressure (SLP), and subsidence were linked to the large-scale ocean-atmosphere circulation associated with PDV and consistent with a positive feedback between low clouds in the eastern subtropical Pacific and the large-scale ocean and atmospheric circulation in the Pacific. For a cool (warm) PDV SST pattern, the authors found an associated strengthening (weakening) in the Pacific Walker circulation, a weaker (stronger) Aleutian Low, and stronger (weaker) climatological subtropical high. These changes were shown to affect the strength of the trades by enhancing (reducing) northerly and easterly flow leading to cooler (warmer) SSTs and enhanced (reduced) LTS and subsidence.

Unfortunately, there is still a great deal of uncertainty in the simulation of low clouds in global coupled General Circulation Models (GCMs) used to study decadal variability and climate change [*Bony and Dufresne*, 2005; *Soden and Held*, 2006; *Clement et al*., 2009]. With the clear economic and societal implications associated with the recent transition of the PDV, the search for a better understanding of the role of low clouds in simulated PDV and the mechanisms for its persistence has become a topic of great interest. In this modeling study, we investigated the influence of observed changes in CRE associated with changes in low cloud amount over recent decades on coupled ocean-atmosphere interactions in the Pacific. To that end, we prescribed observed estimates of shortwave cloud radiative effect (SWCRE) in the eastern subtropical Pacific associated with the most recent PDV transition into a fully coupled GCM. We examined the large-scale ocean and atmospheric response with a particular focus on precipitation over the Americas. We also examined the surface heat budget in the region of the prescribed forcing and remotely to identify potential feedback mechanisms and the role of ocean dynamics in the equilibrium response.

2. Model Description, Data, and Methodology

Our principal source of data is monthly mean gridded low-level cloud amount and surface radiative fluxes from the International Satellite Cloud Climatology Project (ISCCP) [*Zhang et al*., 2004]. Before using ISCCP data, we applied some adjustments to remove spurious long-term variability caused by satellite artifacts and to account for erroneous retrievals of low-level cloud top height [see *Clement et al*., 2009; *Norris and*

Evan, 2015]. Cloud radiative effect (CRE) is defined here as the difference between the all-sky and clear-sky net radiative fluxes. For low clouds in the eastern subtropical Pacific the SWCRE is the dominant term and the net CRE is negative, indicating that an increase in low cloud amount will decrease the amount of radiation reaching the surface. Hence, a more positive (negative) SWCRE is associated with an increase (decrease) in the amount of SW radiation reaching the surface. Other climate variables used in the analysis are Clouds and the Earth's Radiant Energy System (CERES) radiative fluxes [*Loeb et al*., 2009], HadISST [*Rayner et al*., 2003], CMAP precipitation [*Xie and Arkin*, 1997], and zonal and meridional winds at 200 mbar from the ERA-interim analysis [*Dee et al*., 2011].

The model used in this study is the Community Climate System Model (CCSM, version 3.0) from the National Center for Atmosphere Research, CCSM3. In this paper we describe results from the T85 version of CCSM3, with grid points in the atmospheric model (Community Atmospheric Model version 3 (CAM3)) roughly every 1.4° latitude and longitude and 26 levels in the vertical. The ocean component is a version of the Parallel Ocean Program with a nominal latitude-longitude resolution of 1° (0.5° in the equatorial Tropics) and 40 levels in the vertical. The land surface model is the Community Land Model (CLM, V3), and the elastic-viscous-plastic dynamic and thermodynamic sea ice component is the Community Sea Ice Model V4.

Clement et al. [2009] determined that CCSM3 simulated many of the relationships between meteorological quantities (i.e., SST, LTS, and SLP) and low cloud in the northeast subtropical Pacific in a consistent fashion with observations and reanalysis products. An analysis of CRE in the control simulation (CNTRL) shows that area averaged net CRE in CCSM3 in the northeast subtropical Pacific (NESP) index region is $-37\,\mathrm{Wm}^2$ ($-64\,\mathrm{Wm}^2$ SWCRE and $28\,\mathrm{Wm}^2$ longwave cloud radiative effect (LWCRE)). For CERES-computed CRE the area averaged net CRE is quite similar at $-34\,\mathrm{Wm}^2$ ($-61\,\mathrm{Wm}^2$ SWCRE and $26\,\mathrm{Wm}^2$ LWCRE). The prominent role of SWCRE in the eastern subtropics makes shortwave radiation flux at the surface the logical choice to use to introduce a forcing designed to understanding the influence of changes in low cloud on the coupled system.

The modeling approach for this study involves an intervention step in the coupled GCM protocol that allows for the addition of an anomalous flux of, in this case, shortwave radiation into the fully coupled simulation. In this configuration, the SWCRE flux *forcing* (derived from ISCCP) is passed to the ocean component from the coupler in addition to the SW flux calculated by the atmospheric model component. Since the anomalous SW flux *forcing* is introduced after the atmospheric model time step, the atmospheric model is not directly affected by the prescribed flux. The fluxes determined by the atmospheric component are affected by the *response* of the ocean to the prescribed forcing. The ocean component is directly affected by the anomalous SW flux so that the atmosphere is indirectly affected by the prescribed flux at the following coupling interval. The coupling strategy used here should not be confused with a flux correction used to constrain models to be close to observational estimates and reduce drift. Instead the SW flux here is added to the state-dependent SW flux predicted by the atmospheric component and thus adjusts the flux experienced by the ocean component in a manner similar to anomaly coupling strategies [*Kirtman and Shukla*, 2002].

The forcing pattern used in this study is derived from a regression analysis of ISCCP annual mean net shortwave CRE on SSTAs in the northeast subtropical Pacific or NESP index region (215 W–245 W, 15 N–25 N, see *Clement et al*. [2009]). Figure 1 shows the associated SST anomaly pattern and the component of the SWCRE response used as forcing in the CCSM3 simulations. Note that the patterns in Figure 1 highlight the negative phase of PDV and that the pattern of SWCRE shown in Figure 1 is all one sign and retains only the eastern subtropical component of the observed SWCRE pattern where low clouds (and negative SWCRE) play a dominant role. The current study focuses on the component of the SWCRE directly associated with the low cloud under subsidence and with amplitude comparable to that observed in the millennial regime shift. For the NESP index region, the regression pattern in Figure 1 shows a reduction of $7.6\,\mathrm{Wm}^{-2}$. An epoch difference of ISCCP and European Centre for Medium-Range Weather Forecasts (ECMWF) interim SWCRE for the period (1998:2004)–(1992:1997) gives a similar pattern with a reduction of $\sim 7.8\,\mathrm{Wm}^{-2}$ in the NESP index region and a strong signal confined to northwest South America (not shown).

Two cases were run using the SWCRE pattern shown in Figure 1, one that represents an increase in low cloud (anomalous reduction of SW into the surface, or SWneg) and one representing a decrease in low cloud (SWpos). It is important to note that the SWCRE anomaly pattern is fixed in time and therefore does not have an annual cycle. The forcing as prescribed is designed to simulate the low amplitude (less than one standard

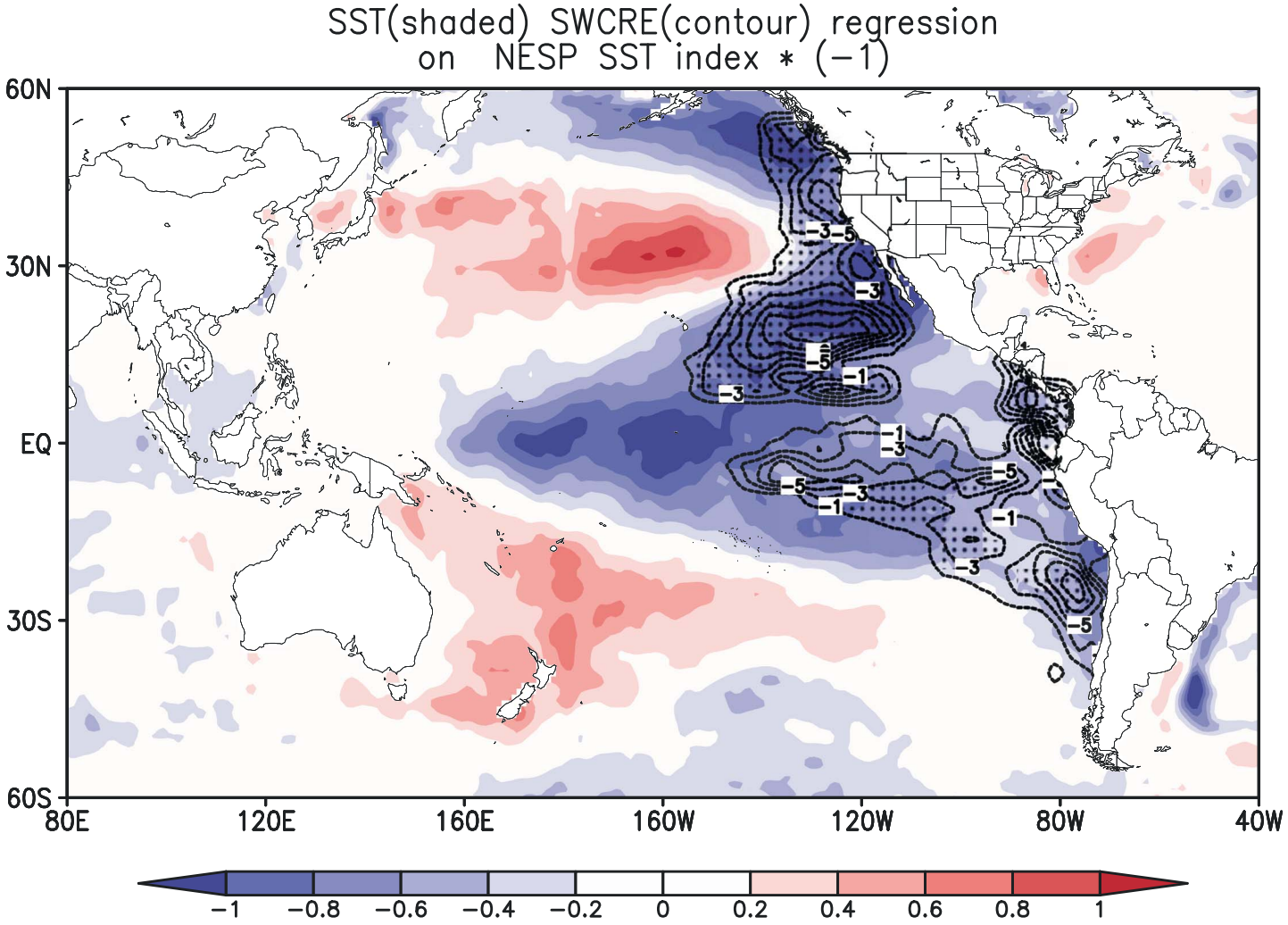

Figure 1. Regression of SST (shaded, °C) and SWCRE (contour, Wm^{-2}) on area averaged SSTAs in NESP index region (215E-245E, 15 N-25 N) multiplied by (−1) to show negative phase.

deviation) observed decadal shifts in the mean low cloud amount. Aside from the prescribed SWCRE forcing the models are fully coupled global simulations and simulate the annual cycle of SWCRE and all other climate variables in response to the persistent forcing. Three ensemble members of each case were run for 40 years, with two of the cases extended to 100 years. Here anomalies describe differences between the 40 year ensemble averages for the case of decreased incident SWCRE (SWneg) with SWpos or a long control simulation (CNTRL). Radiative forcing is fixed and identical in all simulations.

3. Results

Figure 2a shows the epoch difference between HadISST, CMAP precipitation, and ECMWF interim 200 hPa velocity potential (ψ) for a period of increased low cloud amount (1998:2013) and a period with reduced low cloud (1979:1997). The canonical PDV SST pattern is evident, and the epoch difference of 200 hPa ψ shows anomalous ascent over the warm SSTs of the Indonesian subcontinent and enhanced descent in the eastern Pacific, indicating a strengthening of the Pacific Walker circulation. The precipitation pattern in Figure 2a clearly illustrates the shift to more arid conditions in North America and central South American observed since the turn of the century as well as enhanced precipitation over much of the equatorial west Pacific.

Figure 2b shows the 40 year ensemble mean difference between simulated SST, 200 hPa ψ, and precipitation for the SWneg minus SWpos. We note that the spatial characteristics of SWneg-CNTRL are similar, though

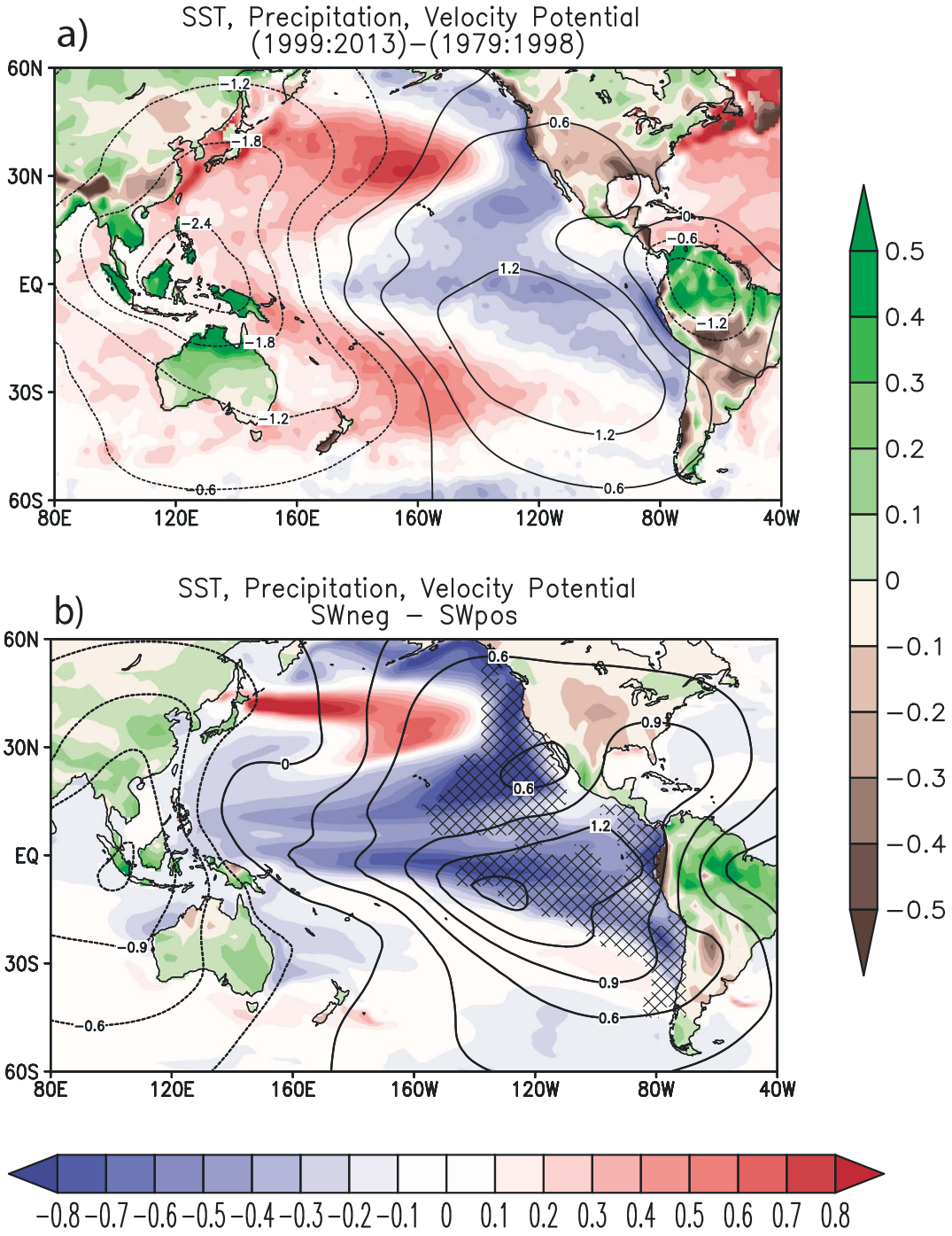

Figure 2. (a) Epoch difference of SST (shaded, °C), precipitation (shaded, mm d^{-1}), and velocity potential (contours, m s^{-1} scaled by 1e06) from observations for the period 1999:2013–1979:1998. (b) Forty year ensemble mean difference between SST (shaded,°C), precipitation (shaded, units mm d^{-1}), and velocity potential (contours, m s^{-1} scaled by 1e06) for SWneg-SWpos. Hatching denotes the region where SWCRE is prescribed.

smaller in amplitude, and the choice of SWneg-SWpos difference shown is convenient for direct comparison of anomalies with observed estimates in Figure 2a. The simulated SSTAs in the tropics extend further west than the observations in Figure 2a, and the warming observed in the western tropical Pacific, South Pacific Convergence Zone, and Indian Ocean is not evident in the simulations. *Deser et al.* [2006] suggested that the simulated westward extent, cold bias, and equatorially confined nature of the Pacific cold tongue in

CCSM3 were also responsible for enhanced El Niño and the Southern Oscillation (ENSO) variability in the western Pacific. Positive SSTAs in the north Pacific associated with the Kurishio extension are more zonally confined than observed, and SST changes in the Atlantic and Indian Oceans are comparatively small.

For the simulated 200 hPa response in Figure 2b, the region of ascent in the west Pacific is shifted to the west and the amplitude is smaller, likely due to the westward extent of cooler SSTs. In the eastern Pacific, the broad pattern of decent is well simulated with relatively (with respect to the west Pacific) strong amplitude though it extends further to the east where the observed North Atlantic warming is not simulated. The simulated precipitation response is weaker with respect to. the amplitude of the simulated SSTs and is characterized by a broad pattern of negative anomalies throughout the contiguous United States, particularly in the region of the Great Plains. In South America, enhanced precipitation over the Amazon Basin and the coastal droughts of Columbia, Ecuador, and Peru are well simulated while the arid conditions to the south have smaller amplitude. It is clear that by introducing the negative SWCRE in the eastern subtropical Pacific with amplitude and sign consistent with the most recent Pacific regime shift, the coupled model response is consistent with the observed shift.

3.1. Surface Radiation Balance

To better understand the large-scale changes shown in Figure 2b, we examine the radiative balance at the surface. In the ocean, outside the forcing region, the local tendency of ocean heat content is balanced by the net downward surface heat flux and the heat carried away by ocean currents (1), where z indicates the depth of the ocean mixed layer. At thermal equilibrium, we can assume that the local tendency of ocean mixed-layer heat content for the control and experimental simulations is equal to 0. Thus, the annual mean of the net downward heat flux will have the same magnitude, but opposite sign, as the inferred annual mean oceanic transport heat divergence (4). Within the forcing region, the SW component in (3) for SWneg and SWpos includes the prescribed SW forcing and the atmospheric model SW response (or feedback).

$$\frac{\partial(HC)}{\partial t} = Q_{\text{net}} + \nabla\cdot\left(\vec{V} * HC\right) \tag{1}$$

$$\text{where } HC = \rho_0 C_p \int_z^0 T(z)dz \tag{2}$$

$$\text{and } Q_{\text{net}} = SW\downarrow - LW\uparrow - SH\uparrow - LH\uparrow \tag{3}$$

$$-Q_{\text{net}} = \nabla\cdot\left(\vec{V} * HC\right) \tag{4}$$

Here we consider the components of the surface heat budget for the NESP index region and for the entire forcing region shown in Figure 1. In the NESP index region, the area averaged SWCRE forcing is $-7.6\,\text{Wm}^{-2}$ in the SWneg simulations. The actual SW that results in the NESP index region, that is, the prescribed forcing plus the AGCM response for the ensemble mean is $-10.9\,\text{Wm}^{-2}$ with respect to CNTRL, indicating a positive SW feedback of $-3.3\,\text{Wm}^{-2}$ or 30% in the NESP index region. Atmospheric damping from longwave radiation ($1.8\,\text{Wm}^{-2}$), sensible ($0.02\,\text{Wm}^{-2}$), and latent heat fluxes ($6.7\,\text{Wm}^{-2}$) account for $8.5\,\text{Wm}^{-2}$ of surface flux in the NESP index region, leaving $2.4\,\text{Wm}^{-2}$ of damping from the (inferred) ocean heat flux divergence (or $-Q_{\text{net}}$, Figure 3c). When the entire forcing region from Figure 3a is considered, the area averaged forcing is $-3.3\,\text{Wm}^{-2}$, the SW feedback remains positive ($-0.65\,\text{Wm}^{-2}$) but is reduced to 16% of the total surface SW ($-3.95\,\text{Wm}^{-2}$) response. Atmospheric damping from longwave radiation ($0.19\,\text{Wm}^{-2}$), sensible ($0.11\,\text{Wm}^{-2}$), and latent heat fluxes ($2.7\,\text{Wm}^{-2}$) account for $3\,\text{Wm}^{-2}$ of surface flux in the NESP index region, leaving $0.95\,\text{Wm}^{-2}$ of damping from the (inferred) ocean heat flux divergence. The atmospheric damping and inferred ocean dynamical response are similar with respect to the total (forcing + feedback) surface SW response for both regions.

The amplitude and extent of the SWCRE forcing (Figure 1a) for SWneg is shown alone in Figure 3a. Figure 3b shows the ensemble mean atmospheric SW response to the prescribed forcing (the SWCRE forcing in Figure 3a is not included) with respect to CNTRL. The SW response is characterized by a large region of negative anomalies in the northeastern subtropical Pacific closely associated with cooler SSTs and increased low cloud amount (defined here as clouds below 700 hPa; not shown). The positive SW anomalies extending from the equatorial west Pacific into the extra tropics are associated with a decrease in midlevel and high-level clouds (not shown).

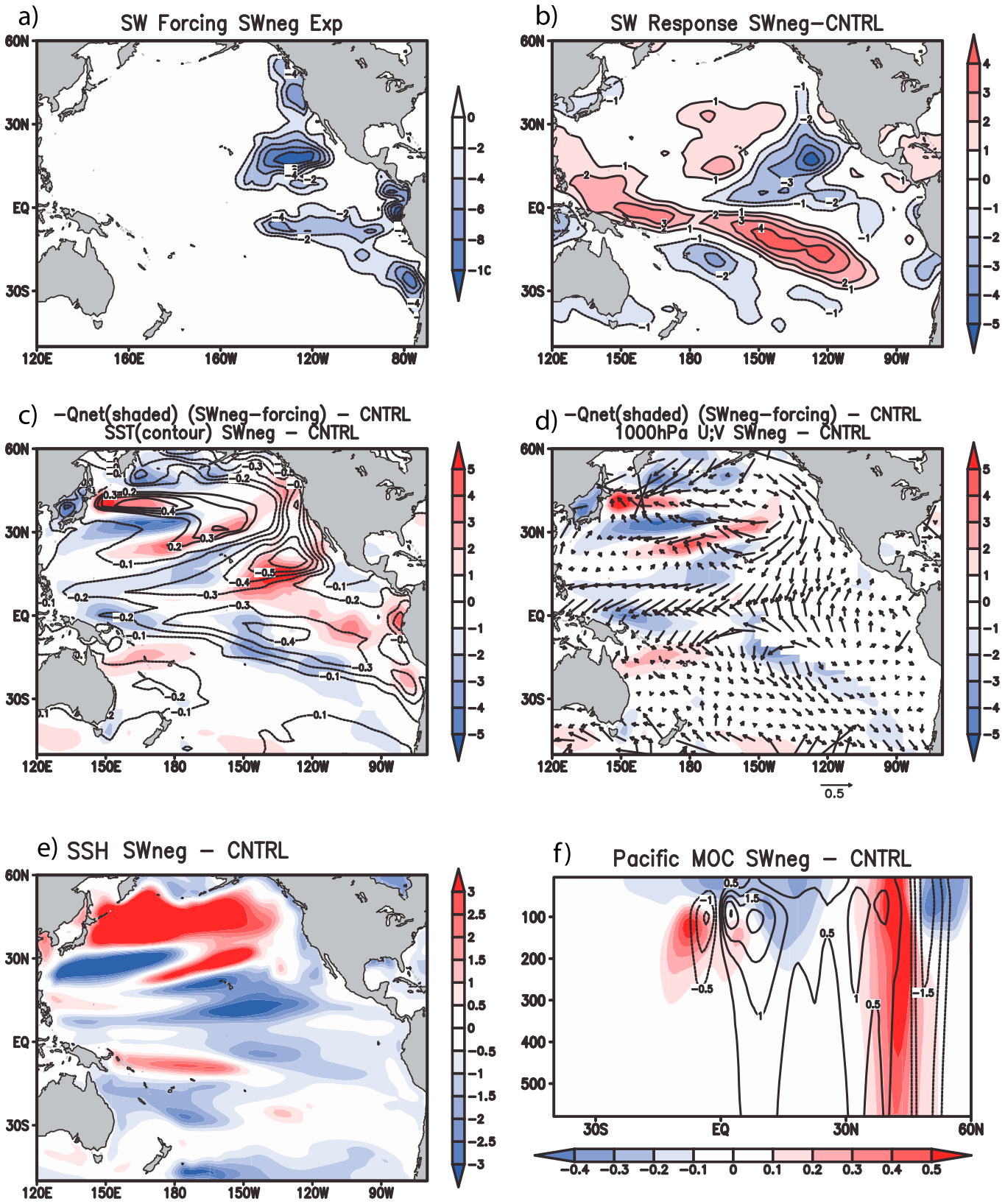

Figure 3. (a) SWneg SWCRE forcing (shaded, units Wm^{-2}), (b) SWneg-CNTRL atmospheric shortwave response (shaded, units Wm^{-2}), (c) surface temperature (contour, units °C) and $-Q_{net}$ (shaded, units Wm^{-2}), and (d) 1000 hPa winds (vectors, units m s^{-1}) and $-Q_{net}$ (shaded, units Wm^{-2}) forcing region masked (e) sea surface height (shaded, units cm), and (f) meridional overturning stream function (contour, SV) and temperature (shaded, units °C).

Figure 3c shows the inferred contribution for ocean heat divergence (or $-Q_{net}$ in (4), in units Wm^{-2}) and SST for SWneg with respect to CNTRL. Note the inclusion of the prescribed negative SWCRE forcing into the SW term in (3) for this calculation. The inclusion of this term provides a simple way to identify the changes in ocean dynamics related to the prescribed forcing in Figure 3a. As stated above, ocean heat divergence in the NESP index region (and forcing region) is positive (read warming) and, thus, acts as a damping term on the anomalously cool SSTs. A similar pattern of SST cooling and strong damping in the northeast subtropics is also present in CNTRL in response to local changes in SWCRE (Figures S1a–S1c in the supporting information). Other noteworthy regions of ocean heat divergence in Figures 3c and S1 include cooling in the equatorial western and central subtropical Pacific and warming in the Kuroshio extension. In Figure 3d, $-Q_{net}$ is shown with the forcing region masked out to highlight where changes in SST and ocean dynamics are not directly influenced by the SWCRE forcing. Figure 3d also includes the changes in the mean surface winds to highlight the role of the large-scale circulation. In the western and central subtropical Pacific, divergence leads to enhanced surface cooling while stronger easterlies throughout the central and western tropical Pacific lead to enhanced transport of warm tropical waters by the Kuroshio and its extension.

Figure 3e shows the difference in sea surface height (SSH) between SWneg and CNTRL. The simulated decrease in SSH in the tropics in consistent with the acceleration of the trade winds shown in Figure 3d, supporting the argument that the large-scale ocean and atmospheric circulation of the Pacific is enhanced in response to the SWCRE forcing in the eastern subtropics. Figure 3f shows the differences in the simulated temperature and meridional overturning circulation (MOC) in the Pacific (120E-270E). Enhanced equatorial trades in the central and western Pacific lead to a cooling of the surface waters and an enhanced meridional overturning circulation with warming in the subsurface waters, particularly in the region of the equatorial undercurrent. In summary, Figure 3 highlights how coupled local and remotely forced feedbacks reinforce the SWCRE forcing in the eastern subtropical Pacific. In the eastern subtropics, cool SSTs feed back directly on low cloud (and SWCRE) via local thermodynamic effects. The large-scale ocean-atmosphere interactions involve local and basin scale changes in the surface winds, vertical overturning circulation, and wind-driven ocean circulation that also act to enhance the eastern subtropical SWCRE forcing. In CCSM3, the regional SWCRE forcing is locally damped by ocean dynamics; however, in the central and western tropical Pacific they are shown to force an enhanced extratropical SLP response that influences surface processes well into the eastern subtropics.

4. Conclusions

In this study, we hypothesize that much of the Pacific basin-wide decadal variability and the associated North American hydroclimate changes can be directly linked to eastern Pacific low cloud variability. This hypothesis that is based on recent research has shown that low cloud amount in the eastern subtropical Pacific is modulated by changes in ocean and atmospheric circulation on decadal timescales [*Deser et al*., 2004; *Burgman et al*., 2008b; *Clement et al*., 2009]. The purpose of this study was to examine the relative roles of local and remote feedbacks and the large-scale ocean-atmosphere interactions in the Pacific linked to low clouds in the eastern subtropics.

Results show that the inclusion of observed estimates of SWCRE, restricted to the eastern subtropical Pacific, into the coupled model framework does a remarkable job of capturing the observed changes in the large-scale oceanic and atmospheric circulation throughout much of the Pacific Basin as well as the associated precipitation changes, particularly in the western hemisphere over the past 16 years. We note here that for the ensemble mean 40 year simulations, there was no significant change in the amplitude or frequency of ENSO, suggesting that the persistence of the PDV pattern played a central role in the arid conditions over the United States in the past 16 years [e.g., *Schubert et al*., 2009; *Burgman and Jang*, 2015]. The simulated increase in precipitation in the western Pacific is also in general agreement with the observations though there are significant differences in the character of the response in Australia, eastern China, and the Tibetan Plateau. This result is consistent with previous studies which showed that changes in the deep-convective forcing in the western Pacific can impact North American hydroclimate via atmospheric teleconnections [*Hoerling et al*., 2001; *Barsugli and Sardeshmukh*, 2002]. The results presented are also consistent with recent studies linking cool SSTs in the eastern Pacific to stronger Walker/Hadley circulations, enhanced ocean circulation

and heat uptake, and reductions in the rate of global warming [*Meehl et al.*, 2011; *England et al.*, 2014; *McGregor et al.*, 2014].

An examination of the surface heat budget identified a strong positive feedback operating between low clouds and SSTs in the northeastern subtropical Pacific. For the NESP index region, where the forcing was strongest, the SW feedback by the atmospheric model contributed 30% to the total local SST cooling. Ocean dynamics in the forcing region worked to damp the local surface cooling particularly in the NESP index region. This was also shown in the CNTRL simulation of CCSM3, suggesting a possible link between ocean dynamics and the limited persistence of simulated SSTs in this region. For the large-scale circulation, locally cooled SSTs increased the SST gradient between the eastern subtropics and the equator, leading to the advection of cool SSTs into the eastern equatorial Pacific. An enhanced zonal SST gradient and stronger trades in the equatorial Pacific resulted in enhanced cooling by ocean dynamics and a strengthening of the subtropical gyre circulation. Stronger trades and enhancing deep convection in the west Pacific also strengthened the atmospheric vertical overturning circulation. In the eastern north Pacific, increased subsidence and SLP weaken the Aleutian low and enhanced the subtropical high resulting in increased cold advection into the subtropics, reinforcing the local thermodynamically induced SWCRE cooling.

In summary, the results suggest a positive feedback that includes locally forced thermodynamic and dynamical changes as well as a remotely forced dynamical atmosphere-ocean component working to enhance the persistence of PDV. For the NESP index region and entire forcing region, ocean dynamics contributed significantly (22% and 24%, respectively) to the local atmospheric damping. However, outside of the forcing region, ocean dynamics enhanced the tropical cooling and strengthen the large-scale circulation. The results presented indicate that the accurate simulation of low clouds in the eastern subtropics, their variability, and persistence on decadal timescales may enhance predictability of near-term (decadal) climate change [*Meehl et al.*, 2014], particularly with respect to persistent shifts in the global mean surface temperature and persistent hydroclimate changes in the Western Hemisphere.

Acknowledgments

We would like to thank the following providers for the data used in our analysis: Radiative fluxes from the ISCCP Project (http://isccp.giss.nasa.gov/), SST from the Met Office Hadley Center (http://www.metoffice.gov.uk/hadobs/hadisst/), Precipitation from the CPC (http://www.cpc.ncep.noaa.gov/products/global_precip/html/wpage.cmap.html), and upper level winds from ECMWF (http://www.ecmwf.int/en/research/climate-reanalysis/era-interim). This study was supported by NOAA grant NA10OAR4310203 and NSF grant 0946225.

References

Barnett, T. P., D. W. Pierce, M. Latif, D. Dommmenget, and R. Saravanan (1999), Interdecadal interactions between the tropics and midlatitudes in the Pacific basin, *Geophys. Res. Lett.*, *26*, 615–618, doi:10.1029/1999GL900042.

Barsugli, J. J., and P. D. Sardeshmukh (2002), Global atmospheric sensitivity to tropical SST anomalies throughout the Indo-Pacific basin, *J. Clim.*, *15*, 3427–3442.

Bellomo, K., A. Clement, T. Mauritsen, G. Rädel, and B. Stevens (2014), Simulating the role of subtropical stratocumulus clouds in driving pacific climate variability, *J. Clim.*, *27*, 5119–5131.

Bony, S., and J.-L. Dufresne (2005), Marine boundary layer clouds at the heart of tropical cloud feedback uncertainties in climate models, *Geophys. Res. Lett.*, *32*, L20806, doi:10.1029/2005GL023851.

Burgman, R., and Y. Jang (2015), Simulated U.S. drought response to interannual and decadal pacific SST variability, *J. Clim.*, *28*, 4688–4705, doi:10.1175/JCLI-D-14-00247.1.

Burgman, R. J., P. S. Schopf, and B. P. Kirtman (2008a), Decadal modulation of ENSO in a hybrid coupled model, *J. Clim.*, *21*, 5482–5500, doi:10.1175/2008JCLI1933.1.

Burgman, R. J., A. C. Clement, C. M. Mitas, J. Chen, and K. Esslinger (2008b), Evidence for atmospheric variability over the Pacific on decadal timescales, *Geophys. Res. Lett.*, *35*, L01704, doi:10.1029/2007GL031830.

Burgman, R., R. Seager, A. Clement, and C. Herweijer (2010), Role of tropical Pacific SSTs in global medieval hydroclimate: A modeling study, *Geophys. Res. Lett.*, *37*, L06705, doi:10.1029/2009GL042239.

Chen, J., A. D. Del Genio, B. E. Carlson, and M. G. Bosilovich (2008), The spatiotemporal structure of twentieth-century climate variations in observations and reanalyses. Part II: Pacific Pan-decadal variability, *J. Clim.*, *21*, 2634–2650.

Chen, X., and J. Wallace (2015), ENSO-like variability: 1900–2013, *J. Clim.*, *28*, 9623–9641, doi:10.1175/JCLI-D-15-0322.1.

Clement, A. C., R. Burgman, and J. R. Norris (2009), Observational and model evidence for positive low-level cloud feedback, *Science*, *325*, 460–464, doi:10.1126/science.1171255.

Clement, A. C., P. DiNezio, and C. Deser (2011), Rethinking the ocean's role in the Southern Oscillation, *J. Clim.*, *24*, 4056–4072, doi:10.1175/2011JCLI3973.1.

Dee, D., et al. (2011), The ERA-Interim reanalysis: Configuration and performance of the data assimilation system, *Q. J. R. Meteorol. Soc.*, *137*, 553–597.

Deser, C., A. S. Phillips, and J. W. Hurrell (2004), Pacific interdecadal climate variability: Linkages between the tropics and the North Pacific during boreal winter since 1900, *J. Clim.*, *17*, 3109–3124.

Deser, C., A. Capotondi, R. Saravanan, and A. Phillips (2006), Tropical Pacific and Atlantic variability in CCSM3, *J. Clim.*, *19*, 2451–2481.

England, M. H., S. McGregor, P. Spence, G. A. Meehl, A. Timmermann, W. Cai, A. Sen Gupta, M. J. McPhaden, A. Purich, and A. Santoso (2014), Recent intensification of wind-driven circulation in the Pacific and the ongoing warming hiatus, *Nat. Clim. Change*, *4*, 222–227, doi:10.1038/nclimate2106.

Galanti, E., and E. Tziperman (2003), A mid-latitude ENSO teleconnection mechanism via baroclinically unstable long Rossby waves, *J. Phys. Oceanog.*, *33*, 1877–1888.

Giese, B. S., S. C. Urizar, and N. S. Fukar (2002), Southern hemisphere origins of the 1976 climate shift, *Geophys. Res. Lett.*, *29*(2), 1014, doi:10.1029/2001GL013268.

Hoerling, M., and A. Kumar (2003), The perfect ocean for drought, *Science*, *299*, 691–694, doi:10.1126/science.1079053.
Jin, F.-F. (2001), Low frequency modes of the tropic ocean dynamics, *J. Clim.*, *14*, 3872–3881.
Jo, H.-S., S.-W. Yeh, and C.-H. Kim (2013), A possible mechanism for the North Pacific regime shift in winter of 1998/1999, *Geophys. Res. Lett.*, *40*, 4380–4385, doi:10.1002/grl.50798.
Kirtman, B. P. (1997), Oceanic Rossby wave dynamics and the ENSO period in a coupled model, *J. Clim.*, *10*, 1690–1704.
Kirtman, B. P., and P. S. Schopf (1998), Decadal variability of ENSO predictability and prediction, *J. Clim.*, *11*, 2804–2822.
Kirtman, B. P., and J. Shukla (2002), Interactive coupled ensemble: A new coupling strategy for CGCMS, *Geophys. Res. Lett.*, *29*(10), 1367, doi:10.1029/2002GL014834.
Kirtman, B., E. Schneider, D. Straus, D. Min, and R. Burgman (2011), How weather impacts the forced climate response, *Clim. Dyn.*, *37*, 2389–2416, doi:10.1007/s00382-011-1084-3.
Kleeman, R., J. P. McCreary, and B. A. Klinger (1999), A mechanism for generating ENSO decadal variability, *Geophys. Res. Lett.*, *26*, 1743–1746, doi:10.1029/1999GL900352.
Klein, S. A., D. L. Hartmann, and J. R. Norris (1995), On the relationships among low-cloud structure, sea surface temperature, and atmospheric circulation in the summertime northeast Pacific, *J. Clim.*, *8*, 1140–1155.
Knutson, T. R., and S. Manabe (1998), Model assessment of decadal variability and trends in the tropical Pacific Ocean, *J. Clim.*, *11*, 2273–2296.
Hamlington, B. D., R. R. Leben, M. W. Strassburg, R. S. Nerem, and K.-Y. Kim (2013), Contribution of the Pacific Decadal Oscillation to global mean sea level trends, *Geophys. Res. Lett.*, *40*, 5171–5175, doi:10.1002/grl.50950.
Hartmann, D. L., M. Ockert-Bell, and M. Michelsen (1992), The effect of cloud type on Earth's energy balance: Global analysis, *J. Clim.*, *5*, 1281–1304.
Hoerling, M. P., J. W. Hurrell, and T. Xu (2001), Tropical origins for recent North Atlantic climate change, *Science*, *292*, 90–92.
Lau, N.-C., and M. J. Nath (1994), A modeling study of the relative roles of tropical and extratropical SST anomalies in the variability of the global atmosphere-ocean system, *J. Clim.*, *7*, 1184–1207.
Loeb, N. G., B. A. Wielicki, D. R. Doelling, G. L. Smith, D. F. Keyes, S. Kato, N. Manalo-Smith, and T. Wong (2009), Toward optimal closure of the Earth's top-of-atmosphere radiation budget, *J. Clim.*, *22*, 748–766, doi:10.1175/2008JCLI2637.1.
Mantua, N. J., S. R. Hare, Y. Zhang, J. M. Wallace, and R. C. Francis (1997), A Pacific interdecadal climate oscillation with impacts on salmon production, *Bull. Am. Meteorol. Soc.*, *78*, 1069–1079, doi:10.1175/1520-0477(1997)078<1069:APICOW>2.0.CO;2.
McGregor, S., A. Timmermann, M. F. Stuecker, M. H. England, M. Merrifield, F.-F. Jin, and Y. Chikamoto (2014), Recent Walker circulation strengthening and Pacific cooling amplified by Atlantic warming, *Nat. Clim. Change*, *4*, 888–892, doi:10.1038/NCLIMATE2330.
McPhaden, M. J., and D. Zhang (2002), Slowdown of the meridional overturning circulation in the upper Pacific Ocean, *Nature*, *415*, 603–608, doi:10.1038/415603a.
Meehl, G. A., J. M. Arblaster, J. T. Fasullo, A. Hu, and K. E. Trenberth (2011), Model-based evidence of deep-ocean heat uptake during surface-temperature hiatus periods, *Nat. Clim. Change*, *1*, 360–364.
Meehl, G. A., et al. (2014), Decadal climate prediction: An update from the trenches, *Bull. Am. Meteorol. Soc.*, *95*, 243–267, doi:10.1175/BAMS-D-12-00241.1.
Norris, J. R., and A. T. Evan (2015), Empirical removal of artifacts from the ISCCP and PATMOS-x satellite cloud records, *J. Atmos. Oceanic Technol.*, *32*, 691–702.
Pierce, D. W., T. P. Barnett, and M. Latif (2000), Connections between the Pacific Ocean tropics and midlatitudes on decadal timescales, *J. Clim.*, *13*, 1173–1194.
Pierce, D. W. (2002), The role of sea surface temperatures in interactions between ENSO and the North Pacific Oscillation, *J. Clim.*, *15*, 1295–1308.
Power, S., T. Casey, C. Folland, A. Colman, and V. Mehta (1999), Inter-decadal modulation of the impact of ENSO on Australia, *Clim. Dyn.*, *15*, 319–324, doi:10.1007/s003820050284.
Rayner, N. A., D. E. Parker, E. B. Horton, C. K. Folland, L. V. Alexander, D. P. Rowell, E. C. Kent, and A. Kaplan (2003), Global analyses of sea surface temperature, sea ice, and night marine air temperature since the late nineteenth century, *J. Geophys. Res.*, *108*(D14), 4407, doi:10.1029/2002JD002670.
Schopf, P. S., and R. J. Burgman (2006), A simple mechanism for ENSO residuals and asymmetry, *J. Clim.*, *19*, 3167–3179, doi:10.1175/JCLI3765.1.
Schubert, S. D., M. J. Suarez, P. J. Pegion, R. D. Koster, and J. T. Bacmeister (2004), Causes of long-term drought in the U.S. Great Plains, *J. Clim.*, *17*, 485–503, doi:10.1175/1520-0442(2004)017,0485:COLDIT.2.0.CO;2.
Schubert, S. D., et al. (2009), A U.S. CLIVAR project to assess and compare the responses of global climate models to drought-related SST forcing patterns: Overview and results, *J. Clim.*, *22*, 5251–5272, doi:10.1175/2009JCLI3060.1.
Seager, R., N. Harnik, Y. Kushnir, W. Robinson, and J. Miller (2003), Mechanisms of hemispherically symmetric climate variability, *J. Clim.*, *16*, 2960–2978, doi:10.1175/1520-0442(2003)016,2960:MOHSCV.2.0.CO;2.
Seager, R., Y. Kushnir, C. Herweijer, N. Naik, and J. Velez (2005), Modeling of tropical forcing of persistent droughts and pluvials over western North America: 1856–2000, *J. Clim.*, *18*, 4065–4088.
Seager, R., Y. R. Burgman, Y. Kushnir, A. Clement, E. Cook, N. Naik, and J. Miller (2008), Tropical Pacific forcing of North American medieval megadroughts: Testing the concept with an atmosphere model forced by coral-reconstructed SSTs, *J. Clim.*, *21*, 6175–6190, doi:10.1175/2008JCLI2170.1.
Soden, B. J., and I. M. Held (2006), An assessment of climate feedbacks in coupled ocean–atmosphere models, *J. Clim.*, *19*, 3354–3360.
Trenberth, K. E., and J. W. Hurrell (1994), Decadal atmospheric–ocean variations in the Pacific, *Clim. Dyn.*, *9*, 303–319, doi:10.1007/BF00204745.
Trenberth, K. E., G. W. Branstator, D. Karoly, A. Kumar, N.-C. Lau, and C. Ropelewski (1998), Progress during TOGA in understanding and modeling global teleconnections associated with tropical sea surface temperatures, *J. Geophys. Res.*, *103*(special TOGA issue), 14,291–14,324, doi:10.1029/97JC01444.
Wang, C., and R. H. Weisberg (1998), Climate variability of the coupled tropical-extratropical ocean-atmosphere system, *Geophys. Res. Lett.*, *25*, 3979–3982, doi:10.1029/1998GL900082.
Wood, R., and C. S. Bretherton (2006), On the relationship between stratiform low cloud cover and lower-tropospheric stability, *J. Clim.*, *19*, 6425–6432.
Xie, P., and P. A. Arkin (1997), Global precipitation: A 17-year monthly analysis based on gauge observations, satellite estimates, and numerical model outputs, *Bull. Am. Meteorol. Soc.*, *78*, 2539–2558.
Yeh, S.-W., and B. P. Kirtman (2006), Origin of decadal El Niño–Southern Oscillation-like variability in a coupled general circulation model, *J. Geophys. Res.*, *111*, C01009, doi:10.1029/2005JC002985.
Zhang, Y., J. M. Wallace, and D. S. Battisti (1997), ENSO-like interdecadal variability: 1900–93, *J. Clim.*, *10*, 1004–1020.
Zhang, Y.-C., W. B. Rossow, A. A. Lacis, V. Oinas, and M. I. Mishchenko (2004), Calculation of radiative fluxes from the surface to top of atmosphere based on ISCCP and other global data sets: Refinements of the radiative transfer model and the input data, *J. Geophys. Res.*, *109*, D19105, doi:10.1029/2003JD004457.